Metrics for Diagnosing Negative Mass and Stiffness when Uncoupling Experimental and Analytical Substructures

Mathew S. Allen
Daniel C. Kammer
Department of Engineering Physics
University of Wisconsin
Madison, WI 53706
msallen@engr.wisc.edu, kammer@engr.wisc.edu

Randy L. Mayes
Structural Dynamics
Sandia National Laboratory
Albuquerque, NM
rlmayes@sandia.gov

ABSTRACT

Recently, a new substructure coupling/uncoupling approach has been introduced, called Modal Constraints for Fixture and Subsystem (MCFS) [Allen, Mayes, & Bergman, *Journal of Sound and Vibration,* vol. 329, 2010]. This method reduces ill-conditioning by imposing constraints on substructure modal coordinates instead of the physical interface coordinates. The experimental substructure is tested in a free-free configuration, and the interface is exercised by attaching a flexible fixture. An analytical representation of the fixture is then used to subtract its effects in order to create an experimental model for the subcomponent of interest. However, it has been observed that indefinite mass and stiffness matrices can be obtained for the experimental substructure in some situations. This paper presents two simple metrics that can be used by the analyst to determine the cause of indefinite mass or stiffness matrices after substructure uncoupling. The metrics rank the experimental and fixture modes based upon their contribution to offending negative eigenvalues. Once the troublesome modes have been identified, they can be inspected and often reveal why the mass has become negative. Two examples are presented to demonstrate the metrics and to illustrate the physical phenomena that they reveal.

1. INTRODUCTION

Component mode synthesis (CMS) has been a fundamental tool for the structural analysis of large complex systems for years. Instead of the system being modeled as a whole, it is broken up into substructures that are then modeled and reduced. This approach is often a necessity due to shear model size, and individual system components are often constructed by different companies. This is especially true in the aerospace community. The Craig-Bampton substructure representation [1] has become the most popular and efficient approach within the aerospace industry. In recent years, there has been a renewed interest in combining analytical based and experimental based substructures using CMS and the imposition of constraints. The direct approach would be to enforce compatibility in the physical connection degrees of freedom between two substructures, but this proves difficult in many problems for several reasons.

Recently, a new approach has been introduced, called Modal Constraints for Fixture and Subsystem (MCFS) [2]. This method reduces ill-conditioning by imposing constraints on substructure modal coordinates instead of the physical interface coordinates. The experimental substructure is tested in a free-free configuration, and the interface is exercised by attaching a flexible fixture, which was dubbed a "transmission simulator" in subsequent works [3]. An analytical representation of the transmission simulator is then used to subtract its effects to produce the desired experimental model of the substructure. This process produces a substructure model that is typically much more accurate than a simple free-free model would be, because of the mass-loading effect of the transmission simulator. However, it has been observed that indefinite mass and stiffness matrices can be obtained for the experimental substructure if the analyst is not careful (e.g. the system has negative mass or stiffness). Similar problems were encountered by other researchers when removing rigid masses from a structure [4]. This paper derives simple metrics that can be used by the analyst to determine which of the systems' modes contribute most to offending negative eigenvalues of either the mass or stiffness matrices. The metrics reveal problems with the subcomponent models that can sometimes be addressed by removing problematic modes or by refining the subcomponent models. Two examples are presented illustrating the metrics and the physics that they reveal.

2. THEORY

2.1. Application of Modal Constraint

The MCFS component mode synthesis approach uses free-free substructure representations, since free-free modal tests are typically more convenient and accurate than the alternatives. In order to properly exercise a substructure during a free-free vibration test, the interface is connected to the transmission simulator [3]. Ultimately this transmission simulator must be subtracted in order to have an experimental representation of the desired substructure. A simple beam example, shown in Fig. 1, will be used to illustrate the process. Component *C* is the system tested to obtain an experimental model, component *A* is a finite element model (FEM) representation of the transmission simulator, and component *B* is the substructure for which an experimental representation is desired. Component *C* is the Combination (hence the letter *C*) of the Base system *B* and the Added transmission simulator *A*, so $C = A+B$. We wish to infer the properties of *B* from the measurements that were acquired on the assembly *C*. The transmission simulator mass-loads the left end of beam *C*, so the model that is obtained for *B* will form a good basis for *B* when it is subsequently assembled to some other structure at the same point (its left end).

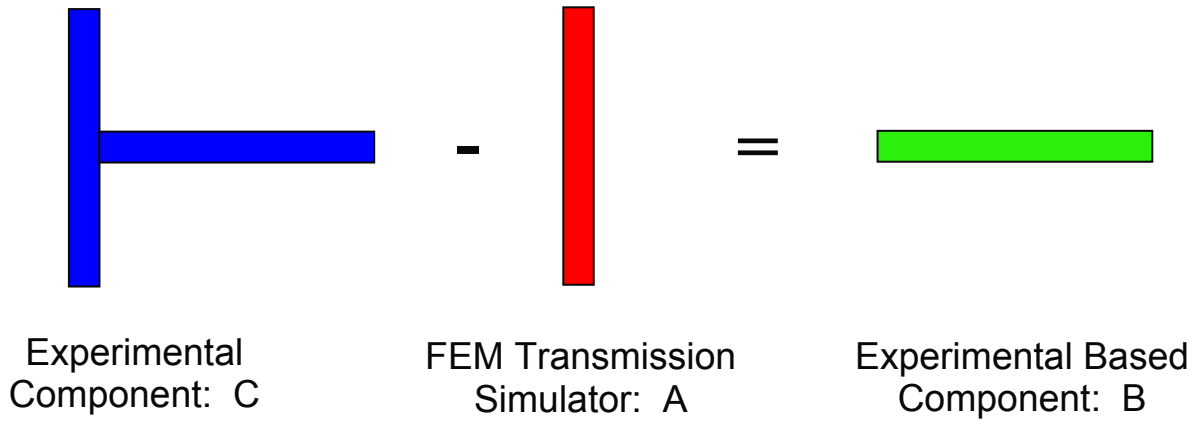

Figure 1: Subtraction of a fixture (or transmission simulator) from an experimental substructure.

The experimental representation of *B* is obtained by coupling *C* and a negative modal representation of *A* (written as B = C-A), which was shown in [2] to cancel the forces exerted by *A* onto *C* under certain basic conditions. The uncoupled equation of motion in modal coordinates is given by

$$\begin{bmatrix} \omega_C^2 & 0 \\ 0 & -\omega_A^2 \end{bmatrix} \begin{Bmatrix} q_C \\ q_A \end{Bmatrix} - \omega^2 \begin{bmatrix} I_C & 0 \\ 0 & -I_A \end{bmatrix} \begin{Bmatrix} q_C \\ q_A \end{Bmatrix} = \begin{Bmatrix} \phi_C{}^{\mathrm{T}} f_C \\ \phi_A{}^{\mathrm{T}} f_A \end{Bmatrix} \tag{1}$$

where ω_C is a diagonal matrix of n_C experimentally derived modal frequencies for component *C,* and ω_A is a diagonal matrix of n_A transmission simulator frequencies computed from its FEM model. For either system, ϕ denotes a matrix of mass normalized mode shapes and *f* the forces applied at the physical coordinates x.

It is assumed that the response of component *C* is measured at n_m locations during the vibration test. In order to couple component *C* and negative component *A*, the usual approach is to enforce compatible displacements at the interface degrees of freedom. However, in general, it is difficult to place sensors and measure all of the degrees of freedom at the interface, especially the rotations. The next best approach would be to enforce displacement compatibility between the two components at the measured locations,

$$x_{Cm} - x_{Am} = 0 \tag{2}$$

but this leads to several difficulties due to measurement errors at the measurement points. An alternative emerges after transforming to modal coordinates,

$$\phi_{Cm} q_C - \phi_{Am} q_A = 0 \tag{3}$$

where ϕ_{Cm} and ϕ_{Am} are the measured partitions of the experimental and transmission simulator components, respectively. Equation (3) can be solved for the transmission simulator modal response

$$q_A = \left[\phi_{Am}^T \phi_{Am} \right]^{-1} \phi_{Am}^T \phi_{Cm} q_C = \phi_{Am}^{\dagger} \phi_{Cm} q_C \tag{4}$$

in which $\phi_{Am}^{\dagger}$ is the left generalized inverse of the transmission simulator modes at the measurement locations. This solution requires that the transmission simulator modal partition at the measurement degrees of freedom be full column rank, which implies that $n_m \geq n_A$. The modal coordinates cannot be directly measured, so these constraints must be written in terms of the physical coordinates before they can be implemented. Premultiplying (4) by ϕ_{Am} and then transforming back into physical coordinates produces

$$x_{Am} = \phi_{Am}\phi_{Am}^{\dagger}x_{Cm} = P_{Am}x_{Cm} = \hat{x}_{Cm} \tag{5}$$

where P_{Am} is an orthogonal projector onto the column space of ϕ_{Am}, and $\hat{x}_{Cm}$ is then the orthogonal projection of the response of substructure *C* at the measurement locations onto this space. Therefore, the modal constraints used in the MCFS approach do not strictly enforce the constraint in Eq. (3), but instead enforce the least-squares fit given in Eq. (5). The best synthesis result will be obtained if $\hat{x}_{Cm} \approx x_{Cm}$, in which case the columns in ϕ_{Cm} can be written as a linear combination of columns in ϕ_{Am}, or $R(\phi_{Cm}) \subset R(\phi_{Am})$.

The modal constraints can be enforced and the constrained generalized coordinates eliminated from eq. (1) with the transformation

$$\left\{ \begin{array}{c} q_C \\ q_A \end{array} \right\} = \left[\begin{array}{c} I_C \\ \tau \end{array} \right] q_C = Tq_C \tag{6}$$

in which $\tau = \phi_{Am}^{\dagger}\phi_{Cm}$. The unforced equation of motion for the reduced or coupled system then has the form

$$m_r\ddot{q}_C + k_r q_C = 0 \tag{7}$$

where

$$m_r = T^T \left[\begin{array}{cc} I_C & 0 \\ 0 & -I_A \end{array} \right] T = I_C - \tau^T\tau \tag{8}$$

and

$$k_r = T^T \left[\begin{array}{cc} \omega_C^2 & 0 \\ 0 & -\omega_A^2 \end{array} \right] T = \omega_C^2 - \tau^T\omega_A^2\tau \tag{9}$$

since the matrices in Eqs. (8) and (9) actually represent approximations for the experimental based substructure *B* mass and stiffness matrices using the modal coordinates of *C* as a basis (see eq. (6) above). The synthesized equation of motion for experimental based substructure *B* is then

$$\hat{m}_B\ddot{q}_C + \hat{k}_B q_C = 0 \tag{10}$$

with

$$\hat{m}_B = I_C - \tau^T\tau \tag{11}$$

and

$$\hat{k}_B = \omega_C^2 - \tau^T\omega_A^2\tau \tag{12}$$

In order for the experimental substructure *B* to be physically realistic, the mass matrix and the stiffness matrix must be positive definite, and positive semi-definite, respectively.

The following section presents an alternative derivation, which shows that the MCFS substructure modal uncoupling technique is equivalent to approximating the transmission simulator mass and stiffness matrices using a SEREP TAM representation [5] for the measured degrees of freedom and then removing the approximated transmission simulator mass and stiffness from a finite element model for *C*. The approach will only be accurate if the modes of the *C* system at all points on the transmission simulator can be accurately represented using the modes of the transmission simulator as a basis. The metrics for ranking the contributions of the subcomponent modes to negative mass and stiffness are presented in Sections 2.3 and 2.4 respectively.

2.2. Alternate Derivation of MCFS Uncoupling by Decomposition

An alternative approach for deriving the relationships for the experimentally based substructure *B* mass and stiffness matrices is based on the more physically intuitive decomposition of substructure *C*. In practice, one does not have a finite element model for C, which is the reason that one is trying to perform experimental substructure uncoupling. However, if the finite element model for *C* were known, its equation of motion in physical coordinates could be written as,

$$M_C \ddot{x}_C + K_C x_C = F_C \tag{13}$$

where the displacement vector can be partitioned into degrees of freedom associated with substructure *A* and substructure *B* as $x_C = \begin{bmatrix} x_{CA}^T & x_{CB}^T \end{bmatrix}^T$. The physical mass matrix M_C can be transformed to modal coordinates using

$$\begin{aligned} m_C &= \begin{bmatrix} \phi_{CA}^T & \phi_{CB}^T \end{bmatrix} \begin{bmatrix} M_{AA} & M_{AB} \\ M_{BA} & M_{BB} \end{bmatrix} \begin{bmatrix} \phi_{CA} \\ \phi_{CB} \end{bmatrix} \\ &= \phi_{CA}^T M_{AA} \phi_{CA} + \phi_{CB}^T M_{BA} \phi_{CA} + \phi_{CA}^T M_{AB} \phi_{CB} + \phi_{CB}^T M_{BB} \phi_{CB} \end{aligned} \tag{14}$$

The mass coupling tends to be small in structural finite element models, so the cross terms are often negligible. (This assumption is not necessary, see the derivation below for stiffness for an alternative.) Neglecting those mass coupling terms, one obtains $m_C = \phi_{CA}^T M_{AA} \phi_{CA} + \phi_{CB}^T M_{BB} \phi_{CB}$ and if the modes are mass normalized the mass matrix of the C system can be written as

$$m_C = I = m_A + m_B \tag{15}$$

in which

$$\begin{aligned} m_A &= \phi_{CA}^T M_{AA} \phi_{CA} \\ m_B &= \phi_{CB}^T M_{BB} \phi_{CB} \end{aligned} \tag{16}$$

are the modal mass representations of substructures *A* and *B* in substructure *C* modal space. Equation (15) can then be written as

$$m_B = I - m_A \tag{17}$$

If one had a finite element model for *C*, the mass matrix for *B* could be computed using these relationships. Of course, if one had a FEM for *C* one could simply delete *A*, but this derivation shows how the models for the subcomponents are related. At this point, one can note a similarity between Eq. (17) and Eq. (11). This reveals that the modal substructuring result produces an estimate of the mass matrix for system A, denoted $\hat{m}_A$, which is given by

$$\hat{m}_A = \tau^T \tau \tag{18}$$

Performing the same analysis for stiffness gives

$$k_C = \omega_C^2 = k_A + k_{AB} + k_{BA} + k_B \tag{19}$$

where

$$\begin{aligned} k_A &= \phi_{CA}^T K_{AA} \phi_{CA} \\ k_{AB} &= k_{BA}^T = \phi_{CA}^T K_{AB} \phi_{CB} \\ k_B &= \phi_{CB}^T K_{BB} \phi_{CB} \end{aligned} \tag{20}$$

In contrast with mass, the stiffness coupling terms k_{AB} and k_{BA} are not zero. Rearranging Eq. (19) produces

$$\hat{k}_B = k_B + k_{AB} + k_{BA} = \omega_C^2 - k_A \tag{21}$$

in which $\hat{k}_B$ is the modal stiffness approximation for substructure *B*. Comparing Eq. (21) with Eq. (12) gives the approximation of the transmission simulator modal stiffness as

$$\hat{k}_A = \tau^T \omega_A^2 \tau \tag{22}$$

To develop the comparison further, consider a finite element model for the transmission simulator, substructure *A*, alone. In physical coordinates, the equation of motion can be written as

$$M_{AA} \ddot{x}_A + K_{AA} x_A = F_A \tag{23}$$

The displacement vector x_A can be partitioned into the measured degrees of freedom and their compliment

$$x_A = \left\{ \begin{array}{c} x_{Am} \\ x_{Ao} \end{array} \right\} \tag{24}$$

The transmission simulator modes can be partitioned in the same manner

$$\phi_A = \left[\begin{array}{c} \phi_{Am} \\ \phi_{Ao} \end{array} \right] \tag{25}$$

Note that that the modal partition ϕ_{Am} was assumed to be full column rank in the previous derivation in Section 2.1. If this is the case, then the physical mass and stiffness matrices in Eq. (23) can be reduced to the measurement degrees of freedom using any of a number of different reduction techniques. This is usually done to generate a reduced mass representation, or test-analysis model (TAM), that is used in test-analysis correlation and analytical model validation [6]. A popular technique for TAM development is called the System Equivalent Reduction Expansion Process (SEREP) [5]. Using this approach, the complete mode shapes of *A* are written in terms of the measured modal partition ϕ_{Am} as

$$\phi_A = T_A \phi_{Am} = \left[\begin{array}{c} \phi_{Am} \phi_{Am}^{\dagger} \\ \phi_{Ao} \phi_{Am}^{\dagger} \end{array} \right] \phi_{Am} = \phi_A \phi_{Am}^{\dagger} \phi_{Am} \tag{26}$$

The reduced mass and stiffness matrices for component *A* at the measurement degrees of freedom are then computed using

$$M_{Ar} = T_A^T M_{AA} T_A \tag{27}$$

$$K_{Ar} = T_A^T K_{AA} T_A \tag{28}$$

It was previously assumed that ϕ_{Cm} can be written as a linear combination of columns in ϕ_{Am}. If this is the case, then ϕ_{Cm} can be written as follows,

$$\phi_{Cm} = \phi_{Am} \gamma \tag{29}$$

where γ is an $n_A \times n_C$ coefficient matrix. Post-multiplying Eq. (26) by γ gives the approximation of the mode shapes of C at all of the points on the transmission simulator, $\hat{\phi}_{CA}$, using the mode shapes of A as a basis.

$$\hat{\phi}_{CA} = \phi_A \gamma = T_A \phi_{Am} \gamma = T_A \phi_{Cm} \tag{30}$$

Substituting Eq. (30) into the first of Eqs. (16) gives the approximation for the transmission simulator modal mass

$$\hat{m}_A = \hat{\phi}_{CA}^T M_{AA} \hat{\phi}_{CA} = \phi_{Cm}^T T_A^T M_{AA} T_A \phi_{Cm} \tag{31}$$

Substituting for transformation T_A from Eq. (26) produces

$$\hat{m}_A = \phi_{Cm}^T \phi_{Am}^{\dagger T} \phi_A^T M_{AA} \phi_A \phi_{Am}^{\dagger} \phi_{Cm} \tag{32}$$

or, assuming modes ϕ_A are mass normalized

$$\hat{m}_A = \phi_{Cm}^T \phi_{Am}^{\dagger T} \phi_{Am}^{\dagger} \phi_{Cm} = \tau^T \tau \tag{33}$$

which agrees with Eq. (18). The corresponding modal stiffness approximation is then

$$\hat{k}_A = \hat{\phi}_{CA}^T K_{AA} \hat{\phi}_{CA} = \phi_{Cm}^T \phi_{Am}^{\dagger T} \phi_A^T K_{AA} \phi_A \phi_{Am}^{\dagger} \phi_{Cm} \tag{34}$$

or

$$\hat{k}_A = \phi_{Cm}^T \phi_{Am}^{\dagger T} \omega_A^2 \phi_{Am}^{\dagger} \phi_{Cm} = \tau^T \omega_A^2 \tau \tag{35}$$

which agrees with Eq. (22). Hence, this analysis has shown that the MCFS substructure modal coupling technique is equivalent to approximating the transmission simulator mass and stiffness matrices using a SEREP TAM representation for the measured degrees of freedom and then removing them from a FEM model for *C*. The accuracy of the approach is dependent upon the accuracy of the approximation $\phi_{CA} \approx \hat{\phi}_{CA}$.

2.3. Ranking Modes based on Mass Approximation

Given a set of experimental modes for substructure *C* and a set of analytical modes for transmission simulator *A*, it is desirable to determine how each mode contributes to negative mass and stiffness in the estimate for *B*. Once the modes that contribute most have been identified the problem can be remedied as discussed in Section 3, sometimes by simply removing them from the model for *C*. From the previous analysis, the approximation for the mass matrix of substructure *B* is given by $\hat{m}_B = I - \hat{m}_A$, where the transmission simulator mass is approximated by $\hat{m}_A = \tau^T \tau$. Matrix τ has dimension $n_A \times n_C$ and was previously shown to have the form

$$\tau = \phi_{Am}^{\dagger} \phi_{Cm} = \left[\phi_{Am}^T \phi_{Am} \right]^{-1} \phi_{Am}^T \phi_{Cm} \tag{36}$$

Prior to ranking modes, it is interesting to develop a better understanding of what matrix τ represents. It was previously illustrated that for the MCFS synthesis method to be accurate,

the experimental modes at the measurement locations for substructure C, ϕ_{Cm}, must lie in the range space of the transmission simulator modes at the same measurement locations, ϕ_{Am}. As mentioned previously, if this is the case then one can write the modes of C as linear combinations of the modes of A using $\phi_{Cm} = \phi_{Am}\gamma$, where γ is the corresponding coefficient matrix. Premultiplying this expression by the generalized inverse of ϕ_{Am} gives

$$\phi_{Am}^{\dagger}\phi_{Cm} = \phi_{Am}^{\dagger}\phi_{Am}\gamma = \gamma \tag{37}$$

and since $\tau = \phi_{Am}^{\dagger}\phi_{Cm}$, τ and γ can be interchanged and one can write,

$$\phi_{Cm} = \phi_{Am}\tau \tag{38}$$

A least squares solution for τ gives back the expression in Eq. (36). If this solution is then substituted into Eq. (38), the result is

$$\hat{\phi}_{Cm} = \phi_{Am}\left[\phi_{Am}^{T}\phi_{Am}\right]^{-1}\phi_{Am}^{T}\phi_{Cm} = P_{Am}\phi_{Cm} \tag{39}$$

which is consistent with Eq. (5). Therefore, the use of τ in the MCFS synthesis approach produces an approximation of the substructure C experimental modes at the measurement locations, $\hat{\phi}_{Cm}$, which minimizes the norm of the error, $e = \phi_{Cm} - \hat{\phi}_{Cm}$. Matrix τ then just represents the linear combination of transmission simulator modes that produces the best fit to the experimental modes.

As mentioned previously, in order for $\hat{m}_B$ to be a physically meaningful representation of the mass of substructure B, it must be positive definite, meaning its eigenvalues must be positive. This then implies that the eigenvalues of $\hat{m}_A = \tau^T\tau$ must be less than 1.0, which implies that the singular values of τ must be less than 1.0. This condition may or may not be satisfied, depending on several factors. In the event that this is not satisfied, one would like to determine which modes of the subcomponents are causing the mass matrix to become negative. The following subsections present methods for ranking the contribution of each subcomponent mode to the negative mass or stiffness. These methods are loosely based on the Effective Independence method for ranking sensor locations in vibration testing [7].

2.3.1. Rank Substructure C Experimental Modes

In this subsection, it is assumed that there is a given set of transmission simulator modes to be used in the construction of τ. The objective is to determine the contribution of the experimental modes of substructure C to the singular values of τ, such that experimental modes can be included or excluded, depending on their contributions to singular values greater than 1.0.

Define the $n_A \times n_A$ matrix $Q_{CM} = \tau\tau^T$. Let L_{CM} represent a diagonal matrix of the eigenvalues of Q_{CM} sorted in descending order, and let Ψ_{CM} be the corresponding eigenvectors. Note that the eigenvalues of Q_{CM} are the squares of the singular values of τ. Therefore, determining the contributions of the experimental modes to the eigenvalues of Q_{CM} is equivalent to determining their contributions to the singular vales of τ. Define the expression

$$e_{CM} = \left[\tau^T \Psi_{CM} \right]^{\wedge 2} \tag{40}$$

where $[\ ]^{\wedge 2}$ represents a term-by-term square. Each row represents one of the substructure C experimental modes, and each column represents one of the eigenvalues of Q_{CM}. It was shown in [7] that each column of e_{CM} adds to the corresponding eigenvalue of Q_{CM}. Therefore, term e_{CMij} gives the contribution of the ith experimental mode of substructure C to the jth eigenvalue of Q_{CM}. If e_{CM} is normalized with respect to the eigenvalues of Q_{CM}

$$e_{CMn} = \left[\tau^T \Psi_{CM} \right]^{\wedge 2} L_{CM}^{-1} \tag{41}$$

then term e_{CMnij} gives the fractional contribution of the ith experimental mode of substructure C to the jth eigenvalue. Using Eqs. (40) and (41), experimental modes that contribute significantly to offending eigenvalues of Q_{CM} can be identified for possible omission from the C mode set. However, it is important to note that while e_{CMij} gives the contribution if the ith C mode to the jth eigenvalue of Q_{CM} for the current mode set, deleting this mode does not mean that the corresponding eigenvalue will be reduced by this amount. As a mode is deleted, the matrix Q_{CM} must be recomputed for the new mode set, which in general may have different eigenvalues with a different distribution over the remaining modes. Therefore, once identified modes are deleted from the C mode set, the eigenvalues of the new matrix Q_{CM} must be calculated to make sure they are less than 1.0.

2.3.2. Rank Substructure A Finite Element Model Modes

In this subsection, it is assumed that there is a given set of experimental modes for substructure C to be used in the construction of τ. The objective is to determine the contribution of the transmission simulator modes, substructure A, to the singular values of τ, such that transmission simulator modes can be included or excluded, depending on their contributions.

Analogous to the previous subsection, define the $n_C \times n_C$ matrix $Q_{AM} = \tau^T \tau = \hat{m}_A$. Let L_{AM} represent a matrix of the eigenvalues of Q_{AM} sorted in descending order, and let Ψ_{AM} be the corresponding eigenvectors. Note that the eigenvalues of Q_{AM} are also the squares of the singular values of τ. Therefore, determining the contributions of the transmission simulator modes to the eigenvalues of Q_{AM} is also equivalent to determining their contributions to the singular values of τ. As before, define the expression

$$e_{AM} = \left[\tau \Psi_{AM} \right]^{\wedge 2} \tag{42}$$

Now each row represents one of the substructure A transmission simulator modes, and each column represents one of the eigenvalues of Q_{AM}. Each column of e_{AM} adds to the corresponding eigenvalue of Q_{AM}, so term e_{AMij} gives the contribution of the ith transmission simulator mode to the jth eigenvalue of Q_{AM}. Normalizing with respect to the eigenvalues of Q_{AM} yields

$$e_{AMn} = \left[\tau \Psi_{AM}\right]^{\wedge 2} L_{AM}^{-1} \tag{43}$$

where e_{AMnij} gives the fractional contribution of the *i*th transmission simulator mode to the *j*th eigenvalue. Using Eqs. (42) and (43), transmission simulator modes that contribute significantly to offending eigenvalues of Q_{AM} can be omitted, or the transmission simulator mode set can be truncated such that the resulting eigenvalues of Q_{AM} are less than 1.0.

2.4. Ranking Modes based on Stiffness Approximation

In all of the cases analyzed to date, it has been the mass approximation of substructure *B* that has been most restrictive with respect to the proper sign definiteness of the resulting matrix after subtraction of transmission simulator *A*. However, the stiffness approximation for substructure *B*, $\hat{k}_B = \omega_C^2 - \tau^T \omega_A^2 \tau$, should also be examined to verify positive semi-definiteness. Note that both ω_C and ω_A will in general contain 6 zeros on the diagonal corresponding to rigid body modes. The generalized inverse of the diagonal matrix ω_C then has the simple form

$$\omega_C^{\dagger} = \begin{bmatrix} 0 & 0 \\ 0 & \omega_{Ce}^{-1} \end{bmatrix} \tag{44}$$

in which ω_{Ce} is a diagonal matrix of the elastic experimental frequencies for substructure *C*. The stiffness approximation can then be written as

$$\hat{k}_B = \omega_C \left[I - \omega_C^{\dagger} \tau^T \omega_A \omega_A \tau \omega_C^{\dagger} \right] \omega_C \tag{45}$$

Defining $\tau_K = \omega_A \tau \omega_C^{\dagger}$, Eq. (45) becomes

$$\hat{k}_B = \omega_C \left[I - \tau_K^T \tau_K \right] \omega_C \tag{46}$$

For $\hat{k}_B$ to be positive semi-definite, the matrix $I - \tau_K^T \tau_K$ must be positive definite. This condition has the same form as that used in the mass approximation. The singular values of τ_K must therefore be less than 1.0. As in the case of mass, modes can now be ranked with respect to the substructure *B* stiffness approximation.

2.4.1. Rank Substructure C Experimental Modes

As in the previous case of mass, it is assumed that there is a given set of transmission simulator modes to be used in the construction of τ_K. The objective is to determine the contribution of the experimental modes of substructure *C* to the singular values of τ_K. Define the $n_A \times n_A$ matrix $Q_{CK} = \tau_K \tau_K^T$. Let L_{CK} represent a matrix of the eigenvalues of Q_{CK} sorted in descending order, and let Ψ_{CK} be the corresponding eigenvectors. Analogous to the mass problem, define the expression

$$e_{CK} = \left[\tau_K^T \Psi_{CK} \right]^{\wedge 2} \tag{47}$$

Each row represents one of the substructure *C* experimental modes, and each column represents one of the eigenvalues of Q_{CK}. Each column of e_{CK} adds to the corresponding eigenvalue of Q_{CK}. Therefore, term e_{CKij} gives the contribution of the *i*th experimental mode of substructure *C* to the *j*th eigenvalue of Q_{CK}. The metric can also be normalized as was done for e_{AM} and e_{CM} and used to determine which modes contribute most to the offending eigenvalues of the stiffness matrix.

2.4.2. Rank Substructure A Finite Element Model Modes

One can also rank the modes of the transmission simulator *A* to the offending eigenvalues of the stiffness matrix. The derivation follows the same form as those presented previously with $Q_{AK} = \tau_K^T \tau_K = \hat{k}_A$, resulting in the following metric.

$$e_{AK} = \left[\tau_K \Psi_{AK} \right]^{\wedge 2} \tag{48}$$

3. Numerical Examples

This section applies the proposed metrics to two different systems. The first is an assembly of beams which was studied in a prior publication [8]. Many of the results presented there are repeated here because they are important to illustrate the issues that can arise. The second system is part of the three-dimensional assembly studied in [2], and it illustrates the complexities that can arise in a more complicated problem.

3.1. Two Dimensional T-beam System

Consider the substructure uncoupling problem pictured in Fig. 1, which was described in Section 2. For the following example all of the subcomponents were modeled with finite elements in order to eliminate any measurement uncertainties. Beam *A* was 152 mm long, 25 mm wide and 19 mm thick, while Beam *B* was 305 mm long with the same cross section. The finite element model was set up so that only in-plane motion, both axial and bending, was possible. The mesh for beams *A* and *B* consisted of 21 and 30 nodes respectively.

The first fifteen modes of *C* will be used in the uncoupling, corresponding to a modal test in which all modes out to 20kHz have been extracted. Each system has three rigid body modes with zero natural frequencies and the natural frequencies of the elastic modes are shown in Table 1. The corresponding mode shapes are not shown, but the lower modes were all observed to involve bending of the horizontal beam, *B*, while the vertical one (transmission simulator *A*) undergoes rigid body rotation. Some of the higher frequency modes show the horizontal beam vibrating axially as the transmission simulator bends. The first six free-modes of *A* are used in the transmission simulator model, three of which are rigid body modes, the 4th and 5th involve bending of beam *A* and mode 6 involves axial motion of beam *A*. Six modal constraints are used to join the negative transmission simulator *A* to *C*. Displacement in both the axial and bending directions at all 21 nodes of the finite element model of *A* are used in forming the modal constraints, although in an experiment one would likely not have such a detailed set of measurements. The rotations at those nodes are not used, since one cannot usually measure rotations in practice.

Table 1 shows the natural frequencies of the *B* system estimated by the modal substructure uncoupling procedure. The actual FEA natural frequencies of the *B* system are also

shown as well as the percent difference. All of the natural frequencies below 17kHz are very accurately predicted, having less than 3% error. However, the modal substructuring procedure returns three natural frequencies which are purely imaginary and do not correspond to any of the analytical natural frequencies. Recall that the negative transmission simulator model is still part of the B system even after substructure uncoupling. Its effect is to cancel the force exerted on B by the actual transmission simulator *A* (see [2]), but each of the nodes on the transmission simulator are still valid points on the *B* system and one can determine how the negative transmission simulator moves in each of *B*'s modes. The deformation shape of each of the modes corresponding to the three imaginary natural frequencies was observed and they were found to involve motion primarily on the negative transmission simulator model subsystem *A*; the motion was three orders of magnitude smaller on component *B* in each of these modes. A few FRFs of the *B* system were reconstructed (not shown here) in the axial and bending directions, and they were seen to overlay the analytical FRFs out to 17kHz, confirming that the spurious modes did not have a large effect on the FRFs. In some applications there would be no need to eliminate these spurious modes since they do not seem to affect the model for B. However, one may not always be so fortunate and in any event these spurious modes are problematic since they cannot be imported into most finite element packages.

	Subcomponents		**System B**		
Mode	**$f_{n,A}$**	**$f_{n,C}$**	**MS est. $f_{n,B}$**	**Actual $f_{n,B}$**	**% Error**
4	4326.5	652.3	1083.3	1081.6	0.2%
5	11926.4	1453.6	0+i*1334.2	-	-
6	16853.0	2924.7	2996.4	2981.6	0.5%
7	-	3090.5	5903.3	5845.1	1.0%
8	-	5751.6	8421.5	8422.1	0.0%
9	-	7285.6	0+i*9157.5	-	-
10	-	9251.0	9824.0	9662.5	1.7%
11	-	12615.3	14832.6	14434.8	2.8%
12	-	13919.7	16965.1	16868.9	0.6%
13	-	14950.0	18066.0	20162.6	-10.4%
14	-	16853.0	0+i*20213	25365.3	-
15	-	19507.0	33706.2	26847.1	25.5%

Table 1: Elastic Natural Frequencies (Hz) of Subsystems C and A, and those that result from using MCFS to compute B=C-A. The actual natural frequencies of the FEA model for B are also shown.

The eigenvalues of the mass matrix of *B* that was estimated with the modal substructuring procedure were found and the lowest five were: -0.012, -0.00038, 3.9e-016, 0.0077, 0.074. Two of these are negative and one is practically zero, indicating that the model for *B* is not physically realizable. A model such as this is incompatible with certain solvers in FEA packages (which require positive definite mass), so one would prefer to find a physically realizable approximation to this model.

In order to investigate this further, the source of these negative eigenvalues was investigated using the metrics developed in this paper. The matrix τ was formed and Q_{CM} was found to have two eigenvalues that were slightly greater than one and a third that was almost exactly equal to one. The EFI procedure was used to compute the contribution of each of the modes of *C* to the eigenvalues of the mass matrix. The elements of e_{CM} corresponding to the modes that contributed most to those eigenvalues are shown in the table below. Each column heading gives the corresponding eigenvalue of Q_{CM} (recall that the eigenvalues of $\hat{m}_B$ are one minus the eigenvalues of Q_{CM}), and the e_{CM} values give the contribution of each mode to that eigenvalue. Contributions below 0.01 have been shown with zeros to improve readability.

Mode of C	Contribution to Eigenvalues of Q_{CM}		
	e_{CM} for $\lambda = 1.012$	e_{CM} for $\lambda = 1.00038$	e_{CM} for $\lambda = 1$
14	0	0	1
6	0.77	0	0
5	0	0.38	0
4	0	0.37	0
3	0.08	0.01	0
7	0	0.08	0
9	0.07	0	0
11	0	0.06	0
2	0.02	0.03	0
12	0.04	0	0

Table 2: Contribution, e_{CM}, of each mode of C to the eigenvalues of Q_{CM}.

Several interesting observations can be made. First, mode 14 is entirely responsible for the zero eigenvalue in $\hat{m}_B$. Visual inspection reveals that mode 14 involves purely axial motion of beam *A*. A corresponding mode exists in subsystem *A*, with the exact same natural frequency. That mode was completely unaltered when *A* was joined to *C* since it has a node at the connection point, so essentially the same mode exists in both *A* and *C*. The zero eigenvalue in $\hat{m}_B$ apparently comes about because this mode's mass is entirely removed from *C* by the substructure uncoupling process. Recall from eqs (7-12), that the *B* system has exactly the same number of modes as the *C* system, so if a mode is removed completely from *C* by the uncoupling process then a spurious mode must remain in the model for *B*.

The other two offending eigenvalues are more difficult to interpret. The table shows that the sixth mode of *C* is the dominant contributor to the first negative eigenvalue, contributing 0.77 of the total value of 1.012. Mode 6, shown with a blue line and open circles in Figure 2, involves axial motion of beam *B* and bending motion of beam *A*. As mentioned previously, the lower modes of *C* all exhibit bending motion of *B* with beam *A* undergoing approximately rigid body rotation, so this is the first mode to show significant bending in *A*. The fact that this mode contributes 0.77 of the 1.012 eigenvalue signifies that this mode carries a significant proportion of the mass associated with bending motion of the transmission simulator, mass which must be removed to accurately predict the natural frequencies of *B*. Hence, the uncoupling algorithm is working with regard to this mode so long as the amount of mass subtracted is correct. To diagnose the situation further, the orthogonal projection of *C*'s motion onto the space of *A*'s modes, $\hat{x}_{Cm}$, was found using the orthogonal projector P_{Am} in eq. (5) and it is also shown in Figure 2 with a red line and with dots at each of the node points. The zoom view shows that the reconstructed motion matches the true motion very well; the maximum difference between the two is 1.4%. Hence, it seems that this mode's contribution to Q_{CM} is physical and represents mass that should be removed.

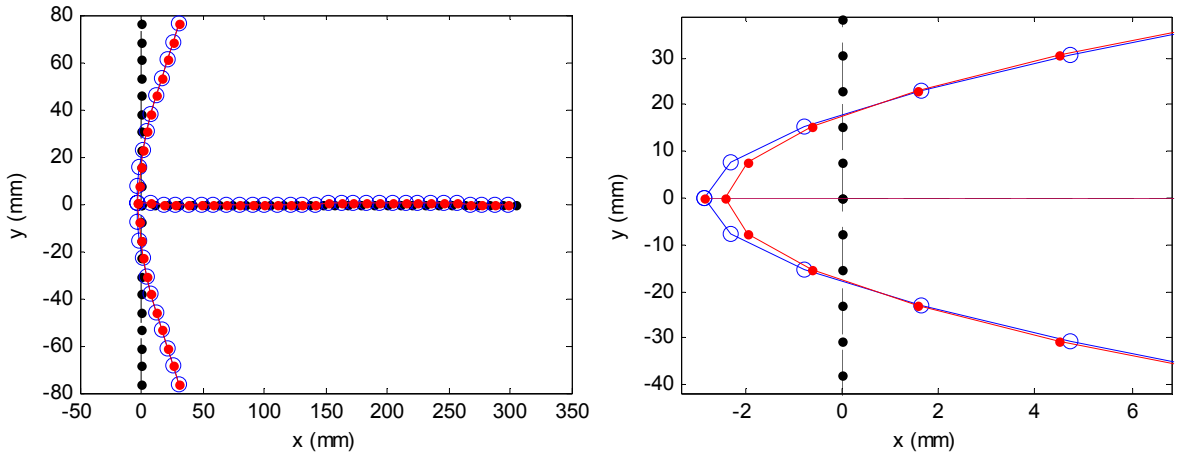

Figure 2: Shape of Mode 6 of system C: (black/dots) undeformed structure, (blue/circles) mode of C, (red/dots) projection, $\hat{x}_{Cm}$, of C onto the free modes of A.

The other mode shapes that contribute to this eigenvalue were also viewed, revealing that there were significant errors when projecting modes 9 and 12 onto the transmission simulator's motion; the maximum difference between the actual motion and the projection was 9.4% and 44.6% respectively. Mode 12's shape is shown in Figure 3 with a blue line. The plot reveals that the 3rd bending mode of the beam would be needed to describe the observed motion, but the model that was used for *A* only included the first two bending modes (and one axial mode). This reveals that the modal basis of the transmission simulator is inadequate to describe mode 12's motion. Because the transmission simulator model does not contain the third bending mode, the uncoupling process might erroneously attribute the third-mode motion to other modes, and hence remove more mass from the first and second bending modes than it should. This might explain why too much mass is removed from the system when the transmission simulator model is subtracted, resulting in negative eigenvalues in the estimated mass matrix. The first eigenvalue of Q_{CM} is 1.012, and the table shows that mode 12 contributes 0.04 to it, so if mode 12 were not present then this eigenvalue might reduce below 1.0 resulting in a positive definite model for *B*.

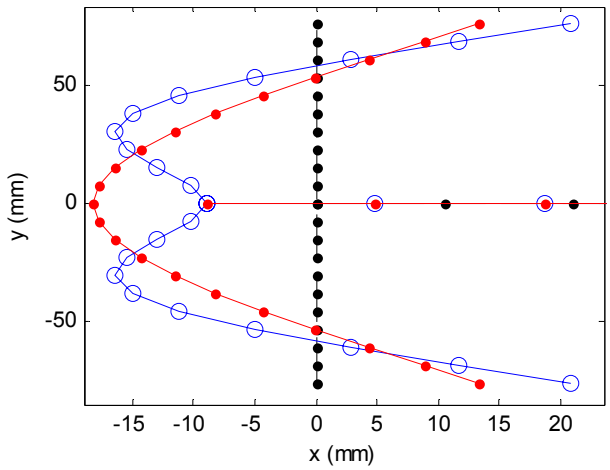

Figure 3: Shape of Mode 12 of system C: (black/dots) undeformed structure, (blue/circles) mode of C, (red/dots) projection, $\hat{x}_{Cm}$, of C onto the free modes of A.

Various modifications to the substructuring process were explored, revealing that the discrepancy in Figure 3 could be reduced greatly by increasing the number of modes in system *A*

to seven. When that was done, the maximum discrepancy between $\hat{x}_{Cm}$ and x_{Cm} was found to reduce from 44.6% to 6.2%. The substructuring calculations were repeated and the corresponding negative eigenvalue of $\hat{m}_B$ had disappeared (although the other remained).

Another alternative would be to reduce the number of modes used in *C* so that the six-mode model for *A* would adequately span the observed motion of *C*. Using six modes for system *A* and eleven modes for system *C*, a positive definite mass matrix was obtained with the smallest eigenvalue being 0.00034. However, since fewer modes were used for *C*, the model obtained for *B* was only accurate up to 14kHz, whereas the FRFs were accurately reconstructed out to 17kHz when 15 modes were used for *C*.

3.2. Three Dimensional Cylinder/Fixture System

The next example considered is one of the system's discussed in [2] where the concept of modal constraints was introduced. Substructure *C*, illustrated in Fig. 1, consists of a hollow cylinder and an attached ring-shaped fixture with tabs. The objective is to obtain an experimental representation of the cylinder alone, substructure *B*, by subtracting off a finite element representation of the fixture (or transmission simulator) using the MCFS approach. For this illustrative example, it is assumed that the response of the cylinder and transmission simulator is measured in three degrees of freedom at 12 points on the transmission simulator, as described in [2]. One hundred modes for substructure *C* were simulated with a finite element model, including six rigid body modes and elastic modes ranging between 433.8 and 6165 Hz. Fifty modes were calculated for the transmission simulator using finite element model, including six rigid body modes and elastic modes ranging between 200.4 and 9,382.0 Hz.

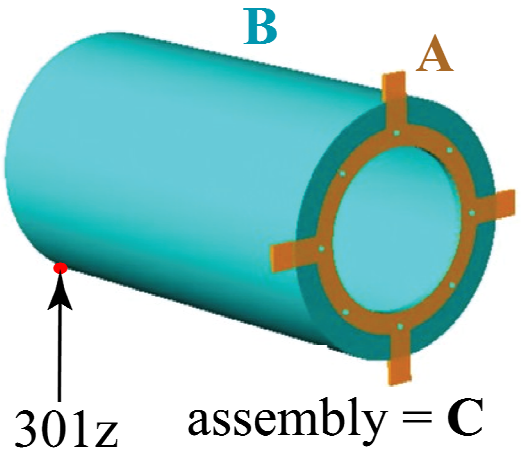

Figure 4: Experimental substructure C consisting of cylinder (B) and transmission simulator (A). Substructure uncoupling will be used to remove the gold colored transmission simulator A from the assembly.

3.2.1. Ranking modes of C

The first application studied is the case where the first 18 modes will be retained for the transmission simulator with frequencies up to 1853.8 Hz and all 100 modes will be included for the composite substructure *C*. When this is done, the mass matrix obtained is not positive definite. The lowest six eigenvalues of the mass matrix are: -0.197, -0.0764, -0.134, -0.118, 0.398 and 0.679. Four of the eigenvalues are below zero, caused by four corresponding eigenvalues of Q_{CM} that are greater than 1.0. The metrics proposed in this paper will be used to rank the *C* modes to determine how they contribute to the mass approximation for substructure *B*. Equation (40) was again used to compute the contributions of the experimental *C* modes to each of the eigenvalues of Q_{CM}. Figure 5 illustrates the cumulative sum over the rows of e_{CM}

for the first six columns corresponding to the six largest eigenvalues of Q_{CM}. The four largest eigenvalues slowly increase in value until the 19th-22nd modes are added, at which point they jump above 1.0 and settle at values between 1.5 and 2.2. In contrast, the fifth and sixth eigenvalues increase slowly over all of the modes always remaining below 0.5.

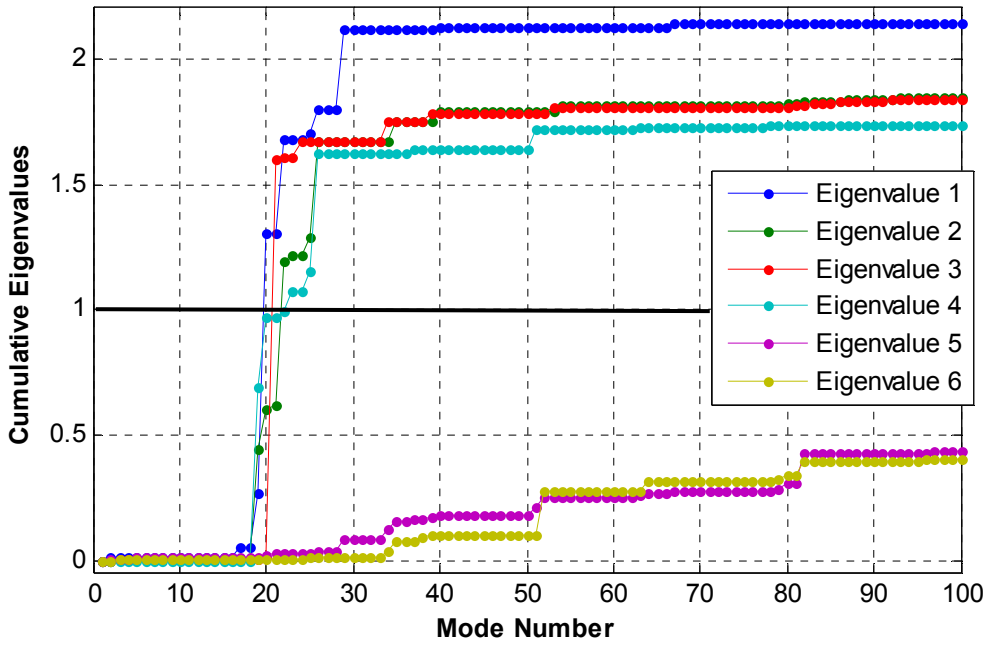

Figure 5: Cumulative sum of eigenvalues of Q_{CM} versus number of modes included in the sum.

The numerical values of e_{CM} are shown in Table 3, in the same format that was used in the previous section. An additional column is also shown that gives the total contribution of each mode to all of the eigenvalues of Q_{CM} that are greater than one (all four that are shown in this case). One observes that mode 21 contributes the most to the large eigenvalues of Q_{CM}, contributing over 86% to the 3rd eigenvalue. The total contributions of modes 19, 20 and 22 make up a similar fraction of the other eigenvalues.

Mode of C	**Eigenvalues of Q_{CM}**				
	Sum	e_{CM} for $\lambda_1 = 2.140$	e_{CM} for $\lambda_2 = 1.845$	e_{CM} for $\lambda_3 = 1.838$	e_{CM} for $\lambda_4 = 1.734$
21	1.60	0	0.01	1.59	0
20	1.48	1.04	0.17	0	0.27
19	1.34	0.21	0.43	0	0.69
22	0.98	0.37	0.58	0	0.03
26	0.95	0.10	0.38	0	0.47
29	0.32	0.32	0	0	0
25	0.17	0.02	0.07	0	0.08
23	0.11	0	0.02	0	0.08
34	0.08	0	0	0.08	0
35	0.08	0	0.08	0	0

Table 3: Contribution, e_{CM}, of each mode of C to the eigenvalues of Q_{CM}.

These results suggest that if modes 19-22 are eliminated from system *C*, then Q_{CM} should be less than 1.0. However, when this is done, one of the eigenvalues remains above 1.0. The 26th mode must also be eliminated from the database to produce a positive definite mass matrix. However, one should not discard modes without cause since they may be important to the model for *B* and to the substructuring predictions obtained with it. To check whether these modes might be important to the model of the cylinder, each mode was plotted. For example, the 20th mode of the *C* substructure is shown in Fig. 6. This and the other mode shape plots reveal that all of the modes in question are dominated by motion of the transmission simulator. The ratio between the maximum displacement of the cylinder part of the structure to the maximum displacement of the transmission simulator was between 4.1% and 10% for these modes. Once the transmission simulator is subtracted, one would expect that this mode might contribute very little to the modal mass of *B*, so small errors and approximation due to the truncated modal basis could cause this mode to have negative mass after substructure uncoupling.

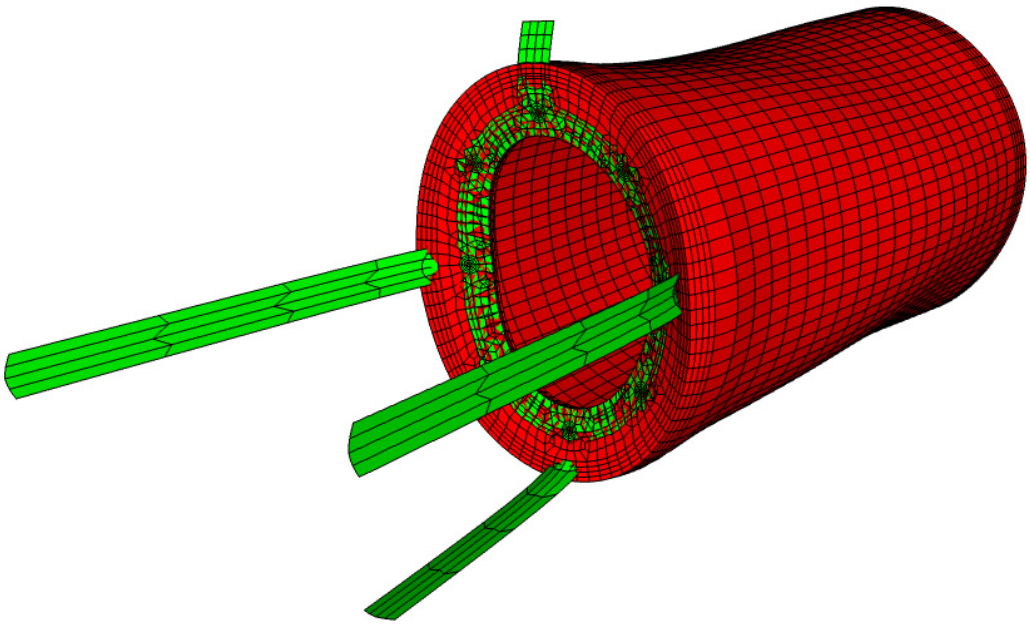

Figure 6: 20th Mode of the Cylinder + transmission simulator.

To see whether these modes were truly insignificant for the substructure model, the full system described in [2] was assembled and its frequency response functions were calculated. Figures 7 and 8 show the drive point FRF of the coupled system at point 301z, which is shown in Fig. 4. Three cases are shown. The solid blue line labeled "analytical" is the FRF of a finite element truth model. The green dashed line is the FRF predicted by substructuring using all of the modes of the cylinder (the C system), and is the same result that was reported in [2]. One can see that the substructuring prediction agrees very well with the truth model. The red dash-dot line is the substructuring prediction obtained after deleting modes 19-22 and mode 26 of the cylinder, as just described. The truncated substructuring prediction also agrees very well with the truth model, except near a few peaks at 1300 and 2300 Hz. The region where the discrepancies occur is magnified in Fig. 8. The FRFs of the system in the axial direction were also shown in [2], but they are not repeated here since there was no discernible difference between the predictions when modes 19-22 and 26 were deleted. These results seem to confirm that these modes are not very important to the subcomponent model. Even then, one would prefer to avoid decreasing the accuracy of the subcomponent model, but for this system none of

these problematic modes can be discarded without degrading the substructuring predictions to some extent at least.

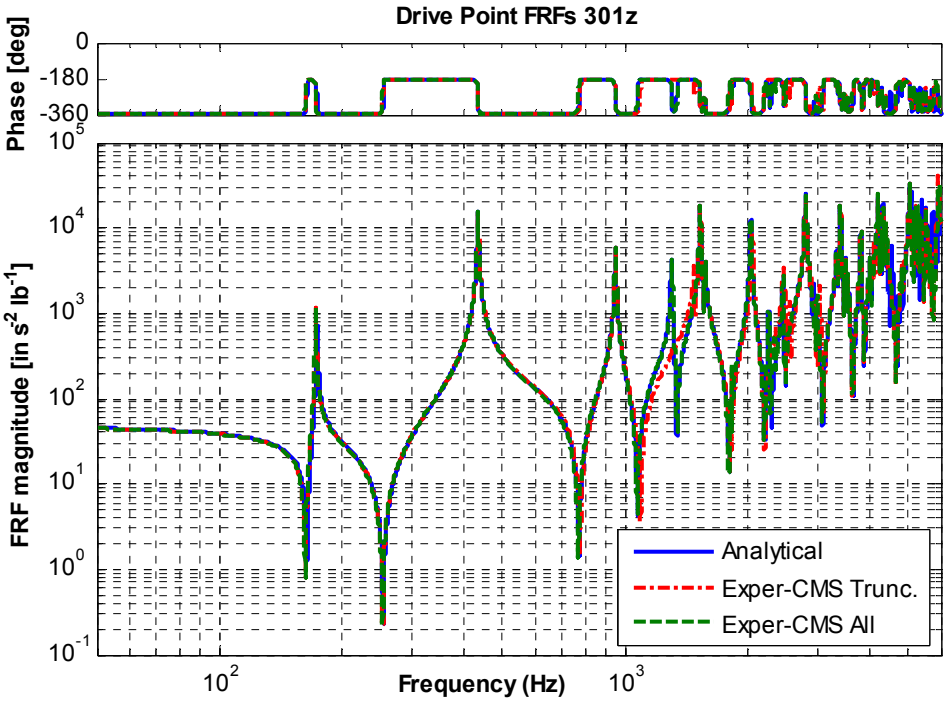

Figure 7: FRF of Cylinder-Plate system described in [2] including all modes of the Cylinder+Transmission simulator ("All") and after eliminating modes 19-22 and 26 ("Trunc.").

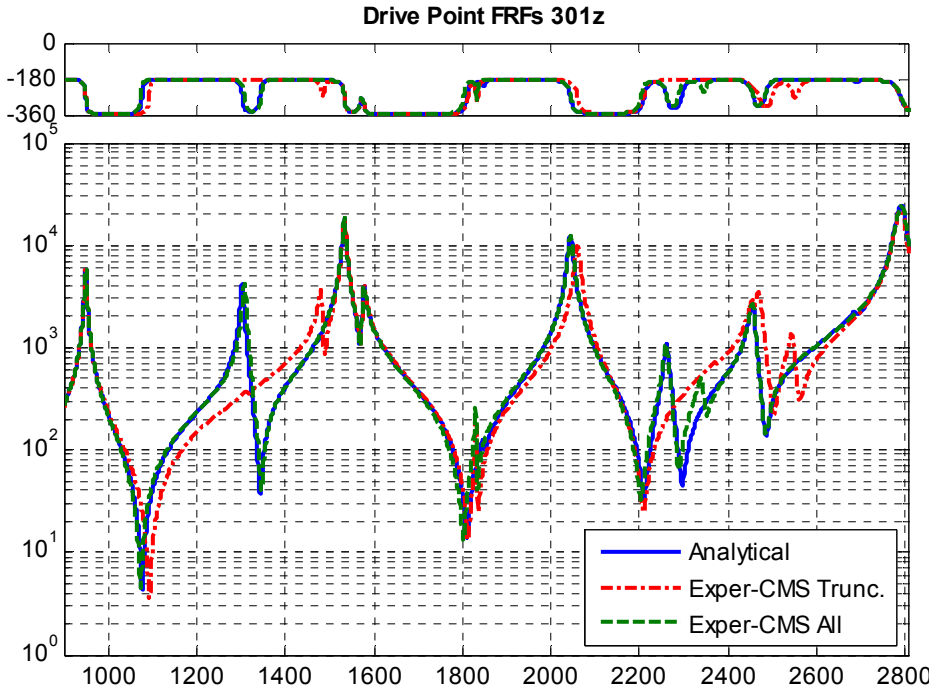

Figure 8: Zoom view of Fig. 7 showing the high frequency region where the substructuring predictions are seen to degrade when modes 19-22 and 26 are excluded from the cylinder model.

3.2.2. Ranking modes of A

For this case the same subcomponents *C* and *A* will be used once again with 100 and 18 modes respectively, only now we shall see how the modes of *A* contribute to the negative

eigenvalues. The eigenvalues of $Q_{AM} = \tau^T \tau = \hat{m}_A$ are the same as those of Q_{CM}. Following the procedure previously outlined, the contributions, e_{AM}, of each of the modes of A to those eigenvalues are shown in Table 4. Modes 9 and 7 contribute significantly to the first and fourth of the eigenvalues of Q_{AM}, but there are a total of seven modes that contribute at least moderately to the negative eigenvalues. There is no justification for removing any of these modes from the model for A, but it is possible that the transmission simulator model is more massive than it should be due to an inaccurate value for its density. To explore this, the modal mass of the seven dominant modes in Table 4 was reduced to attempt to eliminate the negative eigenvalues. Trial and error revealed that the modal mass of these modes had to be reduced to 40% of the original value to obtain a positive definite mass matrix. There does not seem to be a physical justification for such a large reduction; this is a topic of ongoing research. However, it is interesting to note that the substructuring predictions for this system were still very accurate (identical to those shown above and in [2]) even after reducing the modal mass of the transmission simulator so dramatically.

Mode of A	**Eigenvalues of Q_{AM}**				
	Sum	e_{AM} for λ_1=2.140	e_{AM} for λ_2=1.845	e_{AM} for λ_3=1.838	e_{AM} for λ_4=1.734
9	1.42	1.41	0	0	0
7	1.35	0	0.01	0	1.34
6	0.90	0.15	0.47	0.29	0
1	0.88	0.16	0.48	0.23	0
10	0.80	0	0.48	0.32	0
11	0.79	0	0.30	0.49	0
2	0.79	0.37	0	0.42	0
12	0.37	0	0.01	0	0.35
13	0.11	0	0.05	0.03	0.02
14	0.09	0	0.03	0.06	0

Table 4: Contribution, e_{AM}, of each mode of A to the eigenvalues of Q_{AM}.

3.2.3. Ranking modes of C with respect to stiffness

The final application considered is the ranking of the C structure modes based on the stiffness approximation. The case of 18 transmission simulator modes and 100 C modes is again examined. Applying the previously presented procedure, the eigenvalues of $Q_{CK} = \tau_K \tau_K^T$ are computed. In contrast with the mass analysis, all of the eigenvalues of are less than 1.0, therefore the stiffness approximation for substructure B will be positive semi-definite. This is consistent with the authors' experience that the mass approximation of B is usually the most restrictive.

4. CONCLUSION

The Modal Constraints for Fixture and Subsystem method of component mode synthesis has recently been introduced as a means of deriving experimental models of substructures. The experimental substructure is tested in a free-free configuration while the interface is exercised by attaching a flexible fixture or transmission simulator. An analytical representation of the transmission simulator is then used to subtract its effects to produce the desired experimental model of the base structure. It has been observed that indefinite mass and (possibly) stiffness matrices can be obtained in this process. This paper presented simple metrics that can be used by the analyst to determine which modes of each of the subcomponents causes the mass matrix to

become indefinite, by ranking the experimental and transmission simulator modes based upon their contribution to the offending negative eigenvalues.

The metrics were applied to two systems and were found to produce significant insight into the cause of the negative mass. The mass was found to become negative for two reasons: 1.) the system contains modes that are completely removed by the substructuring process leaving mass near zero or 2.) the modal model of the transmission simulator is inadequate to describe the motion of the transmission simulator in the *C* system, leading to inaccuracies that cause too much mass to be removed. The first problem can sometimes be addressed by removing certain modes from the *C* system, although this was found to degrade the substructuring predictions somewhat for the cylindrical system. To address the second problem, one must either increase the number of modes used to describe the transmission simulator A, or reduce the number of modes in *C*.

The metrics presented here can also be used to determine which of the transmission simulator's modes (*A*) contribute most to the negative eigenvalues. Once those modes have been identified, their modal mass can be reduced so that *C* minus *A* does not produce negative mass. One example was presented where the negative mass was eliminated by identifying which transmission simulator modes contributed most to the negative mass and increasing their modal scale factors by 58% (i.e. decreasing their modal mass to 40% of its original value). This was found to produce a physically realizable model, but such a large reduction in modal mass does not seem reasonable. This is just an initial effort into the idea of mass adjustment and further research is needed to understand when this is or is not a viable solution.

The issue of the transmission simulator modes not spanning the space of the modes of *C* was also explored, and the proposed metrics were found to sometimes point to modes for which the span was inadequate. For the beam system, this problem was remedied by increasing the number of modes in the transmission simulator model or by decreasing the number of modes in *C*, although with a consequent reduction in the bandwidth of the model that was obtained for *B*.

The authors suspect that there may be other ways of remedying the problem of negative mass that have not yet been explored. For example, one may find that the transmission simulator model is inaccurate and must be improved before adequate results can be obtained. In any event, the metrics presented in this work should help to guide the analyst to the source of problem so an appropriate solution can be found.

5. ACKNOWLEDGEMENT

This material is based on work supported by Sandia National Laboratories. Sandia is a multi-program laboratory operated by Sandia Corporation, a Lockheed Martin Company, for the United States Department of Energy's National Nuclear Security Administration under Contract DE-AC04-94AL85000.

6. REFERENCES

[1] R. R. Craig and M. C. C. Bampton, "Coupling of Substructures for Dynamic Analysis," *AIAA Journal,* vol. 6, pp. 1313-1319, 1968.

[2] M. S. Allen, R. L. Mayes, and E. J. Bergman, "Experimental Modal Substructuring to Couple and Uncouple Substructures with Flexible Fixtures and Multi-point Connections," *Journal of Sound and Vibration,* vol. 329, pp. 4891–4906, 2010.

[3] R. L. Mayes and M. Arviso, "Design Studies for the Transmission Simulator Method of Experimental Dynamic Substructuring," in *International Seminar on Modal Analysis (ISMA2010)* Lueven, Belgium, 2010.

[4] C. Yasuda, P. J. Riehle, D. L. Brown, and R. J. Allemang, "Estimation Method for Rotational Degrees of Freedom Using a Mass Additive Technique," in *2nd International Modal Analysis Conference (IMAC II)* Orlando, Florida, 1984.

[5] J. O'Callahan, P. Avitable, and R. Riemer, "System Equivalent Reduction Expansion Process," in *7th International Modal Analysis Conference*, Las Vegas, NV, 1989, pp. 29-37.

[6] D. C. Kammer, "Test-Analysis Model Development Using an Exact Modal Reduction," *International Journal of Analytical and Experimental Modal Analysis,* vol. 2, pp. 174-179, 1987.

[7] D. C. Kammer, "Sensor Placement for On-Orbit Modal Identification and Correlation of Large Space Structures," vol. 14, pp. 251-259, 1991.

[8] M. S. Allen, D. C. Kammer, and R. L. Mayes, "Uncertainty in Experimental/Analytical Substructuring Predictions: A Review with Illustrative Examples," in *ISMA2010 - International Conference on Noise and Vibration Engineering* Leuven, Belgium, 2010.